SLAC-PUB-2818
October 1981
(M)

A STUDY OF CATHODE EDGE EMISSION*

Yong-xiang Zhao
Stanford Linear Accelerator Center
Stanford University, Stanford, California 94305

ABSTRACT

A great deal of experimental evidence shows that the perveance of high power klystrons is much higher than normal at low voltage. Thus the three-halves power law is violated in that range. It is hypothesized that this is caused by edge emission. A detailed analysis is given. The calculated magnitude is reasonably coincident with experimental results. The analysis is also valid for other thermionic tubes.

(Submitted to Journal of Applied Physics)

---

*Work supported by the Department of Energy, contract DE-AC03-76SF00515.

INTRODUCTION

The three-halves power law originated by Langmuir and Child is well known as an intrinsic characteristic of a diode or an electron gun operated under space-charge limited condition. However, in practice, this condition is not always satisfied perfectly. According to one theory,[1] when the anode current is close to saturation, the three-halves power law should be replaced by one which exhibits a smooth transition from space-charge limited state to temperature limited state. On the other hand, we found that when the anode current is far lower than saturation, the anode current is always higher than that calculated by the three-halves power law.[2] The lower the anode voltage, the higher the perveance. Some typical experimental performances at low voltage of SLAC's (Stanford Linear Accelerator Center) S-band klystrons (XK-5) are shown in Figs. 1 and 2. Similar performances are also found in other klystrons including those produced by the RCA company.[2] Therefore, one has to consider whether there might exist an extra current other than space-charge limited current. Many possibilities have been considered and excluded. However, it is found that the condition on which the three-halves power law is based is not satisfied for the edge region where there is no or little space charge. Since the thickness of the electron cloud may not be negligible when the anode current is much lower than the emission current, the edge current may become sizeable. This paper is intended to analyze the edge current and explain the abnormal phenomenon.

THE ROLE OF THE ELECTRON CLOUD AND ITS BORDER

It is generally assumed that near the cathode surface there is a layer of electrons, called the electron cloud, in which the space-charge field results in a lower potential relative to the cathode. The potential minimum is referred to as a virtual cathode or a potential barrier. Only those electrons whose initial velocities are high enough can cross the barrier and reach the anode. The higher the barrier, the less the anode current. Therefore, the height of the barrier, or the potential of the virtual cathode, will determine the ratio of the anode current to the emission current.

The virtual cathode is the border of the electron cloud, because the electrons beyond this border are affected by the accelerating field and will never turn back, while the electrons inside this border move randomly in every direction. So this border can be regarded as an emitting surface just like a cathode. The total anode current will be the integral of the emitted current along the whole virtual cathode surface or the border.

Let us now consider the edge of the cathode. Because beyond the edge there is no emission, no or little space charge, the barrier near the edge must be lower than that in the center part as shown in Fig. 3(b). However, since the motion inside the cloud is directed in every direction with the same probability, there must be some electrons moving transversely and crossing the barrier with a higher probability than in the center part. Figure 3(c) shows the current density along the cathode surface. When the height of barrier approaches zero, the current density approaches a temperature limited maximum. The transverse motion of

electrons may also cause the electron cloud to expand transversely, and this implies that the area of the emitting surface is enlarged a little.

Under general conditions, the anode current is so high that this extra current can be neglected. However, when the anode voltage is reduced to such a level that the barrier in the center part is so high that the current emitted from it is very weak, the extra emission may play a significant role. Because the height of the edge barrier always ranges to zero, there are always some electrons escaping from this border no matter how high the barrier in the center part is.

THE EDGE EMISSION CURRENT

In order to estimate the edge emission, we make the following assumptions for the sake of simplicity:

1. The electron initial velocity follows Maxwell's distribution law. This is not exactly true for oxide cathodes; however, the distribution probability decreases approximately exponentially with the velocity, so a Maxwellian distribution will be an approximation.
2. The emission and the field on the surface of the cathode are uniform, and the virtual cathode is very close to the cathode. Thus we can use a one-dimensional approximation except at the edge.
3. The border of the electron cloud on the edge is a straight line as shown in Fig. 4.
4. Inside the electron cloud, the equipotential lines are parallel to the cathode (Fig. 4) instead of perpendicular to the edge as it should be (see Fig. 3(a)).

Suppose the cathode potential is zero, so the potential of the virtual cathode V_m, and V inside the electron cloud are always negative, viz. $V < 0$, $V_m < 0$.

By virtue of the assumptions 1 and 2, one can obtain the following relation[3]:

$$\frac{j_a}{j_e} = e^{\frac{eV_m}{KT}} = e^{-\eta_m} \tag{1}$$

and the potential distribution function is:

$$\xi(\eta) = \int_o^{\eta} \frac{d\eta}{\sqrt{e^{\eta} - 1 + e^{\eta}\,\phi(\sqrt{\eta}) - 2\sqrt{\eta/\pi}}} \tag{2}$$

where j_e is the emission current density, j_a is the anode current density, ξ and η are the normalized coordinate and potential relative to the virtual cathode, on which $\xi = \eta = 0$ (see Fig. 5). η_m is the normalized height of the barrier. ϕ is the error function. They are:

$$\xi = C(z - z_m)$$

$$\eta = \frac{e}{KT}(V - V_m)$$

$$\eta_m = -\frac{eV_m}{KT}$$

$$\phi(t) = \frac{2}{\sqrt{\pi}} \int_o^t e^{-t^2} \cdot dt$$

$$C^2 = \frac{e}{\varepsilon_o} (2\pi m)^{\frac{1}{2}} (KT)^{-\frac{3}{2}} j_e e^{-\eta_m}$$

$$C = 9.2 \times 10^5\, T^{-\frac{3}{4}}\, j_a^{\frac{1}{2}} \quad , \tag{3}$$

where z is the distance from the cathode, z_m is the position of the virtual cathode. The above quantities are dimensionless except C, which has units cm^{-1}. The units of j_a are amp/cm^2, and T, degree Kelvin.

The function (2) is shown in Fig. 6. z_m vs. anode current density j_a as a function of the ratio of the emission current to anode current is shown in Fig. 7.

In addition, the current density crossing the equipotential line with potential V, is:

$$j = j_e e^{\frac{eV}{KT}} = j_e e^{\eta - \eta_m} \quad . \tag{4}$$

Suppose the width of the edge border is W (Fig. 4), then we have:

$$\sin\alpha = \frac{z_m}{W} = \frac{\xi_m}{CW} \qquad (\xi_m = Cz_m) \tag{5}$$

and

$$dW = \frac{dz}{\sin\alpha} \quad .$$

The emission current from an elemental area of the border is only determined by the potential thereof. Therefore:

$$dj_{ed} = j_e e^{\frac{eV}{KT}} \cdot dW$$

$$= j_e e^{-\eta_m} e^{\eta} \frac{dz}{\sin\alpha} \quad . \tag{6}$$

From assumptions 3 and 4, the edge current should be:

$$j_{ed} = \int_o^{z_m} j_e \frac{e^{-\eta_m}}{\sin\alpha} e^{\eta} \, dz = \frac{j_e}{C \sin\alpha} e^{-\eta_m} \int_o^{\xi_m} e^{\eta} \, d\xi \tag{7}$$

Substituting C and sinα one can obtain:

$$j_{ed} = \sqrt{j_e\, j_a}\; W\; f_1(\eta_m)$$

$$f_1(\eta_m) = \frac{e^{-\eta_m/2}\displaystyle\int_o^{\eta_m} \frac{e^{\eta}\, d\eta}{\sqrt{e^{\eta} - 1 + e^{\eta}\,\phi(\sqrt{\eta}) - 2\sqrt{\eta/\pi}}}}{\displaystyle\int_o^{\eta_m} \frac{d\eta}{\sqrt{e^{\eta} - 1 + e^{\eta}\,\phi(\sqrt{\eta}) - 2\sqrt{\eta/\pi}}}} \qquad (8)$$

The numerical solution of the function $f_1(\eta_m)$ is shown in Fig. 8. It shows that $f_1(\eta_m)$ changes not much when η varies over a wide range. It approaches a constant when η is greater than 5, which is generally satisfied at very low voltage.

To evaluate the increment of the anode current due to the edge emission, one should deduct the original anode current emitted from the edge area, which equals $j_a W$. Then one obtains:

$$j'_{ed} = \sqrt{j_e\, j_a}\; W\; f_1(\eta_m) - j_a\, W = \sqrt{j_e\, j_a}\; W\; f_2(\eta_m) \quad , \qquad (9)$$

where

$$f_2(\eta_m) = f_1(\eta_m) - e^{-\eta_m/2} \quad .$$

The function $f_2(\eta_m)$ is also shown in Fig. 8, which is close to a constant when η_m is rather high, or anode voltage is very low, but it drops when η_m is lower (anode voltage is higher).

The total edge current should be a line integral along the circumference of the cathode. It is:

$$I_{ed} = 2\pi R\; j'_{ed} = \sqrt{j_e\, j_a}\; 2\pi R \cdot W \cdot f_2(\eta_m) \quad , \qquad (10)$$

where R is the radius of the cathode.

The anode current emitted from the main part of the cathode is:

$$I_{ao} = \pi R^2 j_a = KV_a^{\frac{3}{2}} \tag{11}$$

Use is made of the assumption 2. The anode current excluding the edge current follows the three-halves power law. K is the perveance of the gun. Then we obtain:

$$I_{ed} = 2\sqrt{\pi}\, W\sqrt{K j_e}\, V_a^{\frac{3}{4}}\, f_2(\eta_m) \quad . \tag{12a}$$

Since η_m is also related to the anode voltage, the above formula can be expressed as a function of anode voltage as follows:

$$I_{ed} = 2\sqrt{\pi}\, W\sqrt{K j_e}\, V_{as}^{\frac{3}{4}}\, f_3\left(\frac{V_a}{V_{as}}\right) \quad . \tag{12b}$$

where

$$V_{as} = \left(\frac{S j_e}{K}\right)^{\frac{2}{3}} \qquad (S = \pi R^2)$$

is the voltage at which the cathode approaches saturation. The function $f_3(V_a/V_{as})$ is shown in Fig. 9. It follows the three-fourths power of the anode voltage rather than the three-halves power when the anode voltage is rather low, but it declines when the edge current density is comparable with the saturation current density.

Another important deduction is that the edge current also depends on the emission density of the cathode. Therefore the edge current might be used as a diagnostic tool of the cathode emission ability.

The ratio of the edge current and normal anode current is

$$\frac{I_{ed}}{I_{ao}} = \sqrt{\frac{j_e}{j_a}}\ \frac{2W}{R}\ f_2(\eta_m) \quad . \tag{13}$$

Since the width of the edge is much less than the radius, generally I_{ed} is negligible. However, when j_a is far less than j_e, the edge current may be substantial, even higher than the normal current I_{ao}.

SPACE CHARGE EFFECT

The total anode current should be determined by solving Poisson's equation combined with the boundary condition at the cathode. Unfortunately, the boundary at the edge is so complex that a rigorous solution is very difficult to perform. Nevertheless, the effect of the space charge of the edge emission has to be considered by all means. As a matter of fact, when the edge emission is significant, its space charge field will result in decreasing the potential on the cathode surface, or elevate the height of the virtual cathode barrier, especially on those areas close to the edge as shown in Fig. 3(b). (The solid lines are higher than the dashed lines.) On the contrary, the anode current emitted from that area is reduced. Therefore, the net increment of the total anode current will be less than the edge emission calculated above.

The current density which crosses the barrier with a normalized height of η_m is

$$j_a = j_e\ e^{-\eta_m} \quad . \tag{14}$$

Suppose the increment of the barrier due to the space charge of the edge current is $\Delta\eta_m$.

$$\eta_m = \eta_{mo} + \Delta\eta_m = \eta_{mo}(1 + \delta) \quad . \tag{15}$$

where the subscript '0' of η_m indicates no edge current being taken into account, and it is related to the three-halves power law as follows:

$$j_{ao} = j_e e^{-\eta_{mo}} = \frac{K}{S} V_a^{\frac{3}{2}} \quad . \tag{16}$$

Substituting (14) through (16) into (10), the formula (12a) is replaced by the following:

$$I_{ed} = \beta j_e^{\frac{1}{2}(1-\delta)} V_a^{\frac{3}{4}(1+\delta)} \quad . \tag{17}$$

where β is an approximate constant at low voltage. Note that the exponent of V_a is changed.

EXPERIMENTS

All the experiments with various tubes show that the perveances at low voltage are higher than the design values. Figures 1 and 2 show some typical low voltage performances of SLAC S-band klystrons, which are normally operated at an anode voltage of about 260kV. At voltages lower than 10V, those data will be inaccurate because the contact potential difference becomes comparable. But if it is taken into account, the perveance should be even higher.

To estimate the quantity of the edge current, suppose V_a = 1000V, $j_e = 10 a/cm^2$, $K = 2 \times 10^{-6} a/V^{3/2}$, I_{ao} = 63 ma, $j_a = 1.2 \times 10^{-3} a/cm$. From Figs. 7 and 8 one obtains $z_m = 1.4 \times 10^{-2}$ cm, $f_2(\eta_m) = 0.55$. Suppose $W = 2z_m$, then we obtain: I_{ed} = 43 ma. This is the same order of magnitude as the extra current we obtained.

Figure 10(a) shows the edge current of Tube M433. It is the difference of the anode current measured and that calculated by the

three-halves power law. Its perveance is measured at high voltage and revised by virtue of the relativistic correction. It exhibits good agreement with the theoretical curve in Fig. 9 and formula (12). It has a slope of about 0.75 on logarithmic paper. Note that this tube is tested before its high voltage RF test, so that its cathode has not been activated completely. Figure 10(b) shows similar performance of a UHF klystron undergoing a reactivation process. It also has inadequate emission.

The performances of two normal tubes (M437 and M388) are shown in Fig. 11. Note that they have much higher edge current than the former, and their slopes are about 1 (between 3/2 and 3/4). This can be explained by formula (17). In all these tubes we can find that the edge current drops down when the filament power is low enough. They exhibit the saturation characteristic as indicated above. (Note that usually in practice the temperature near the edge is lower than that at the center, while the extracted current density is higher due to the nonuniformity, so the outer part of the cathode might be saturated far earlier than that in the center.)

Another interesting fact can be seen from Fig. 12. It shows that a tube has not yet been activated thoroughly after the low voltage aging process, although it follows the three-halves power law. After high voltage RF test, which is in fact a further activation process, the anode current is raised significantly, and the three-halves power law is then violated in the low voltage region. This current increment is edge current and is an indication of the emission ability or the degree of the activity of the cathode as mentioned above.

The practical situation is no doubt more complex than what we have considered here, particularly the state of the electron cloud is not well known. It becomes more complex when a cathode is large so that the temperature as well as the work function are not uniform.

In a real tube the edge of the cathode is not a boundary between two sections of the same plane as in the idealized case (Fig. 3(a)). The variation in minor spacings of an assembled multiple element cathode structure will lead to variations in measured data which might be due to edge effects. Since the edge width W as well as the emission current vary over wide ranges, there is no doubt that the extra current is different from tube to tube.

CONCLUSION

1. The edge current plays an important role at low voltage. The phenomenon that the anode current at the low voltage range is higher than that calculated by the three-halves power law is a natural one.
2. This extra current is a measure of the emission ability of the cathode. It is an indication of the degree of activation during the manufacturing process and the degree of the decay of the cathode during the lifetime of tubes.

Note that the analysis in this paper is only qualitative rather than quantitative. It does not include other possibilities which may also contribute a certain amount of extra current, such as parasitic emission.

In addition, although only klystrons were tested, all the arguments are obviously also valid for other thermionic tubes, especially for O-type microwave tubes such as travelling-wave tubes. Since the subject is only concerned with the gun region where no RF field exists, the individual microwave structure is not a factor affecting the analysis.

ACKNOWLEDGEMENTS

This work was performed under the direction of Dr. G. T. Konrad. The author wishes to express his thanks to many colleagues who helped a great deal in making the experiments possible. Among them are G. Aske, C. Rivers, F. Coffer, C. Griffin and many others. Especially, T. Schumacher helped a lot with the experiments. The author is particularly indebted to Professor M. Chodorow for his enlightening discussion. The author also wishes to express his thanks to T. Lee and E. S. Wu for their beneficial discussions.

This work was supported by the Department of Energy contract DE-AC03-76SF00515.

REFERENCES

[1]R. T. Longo, IEEE International Electron Device Meeting (IEDM) (1978), p. 152; ibid., (1980), p. 467.

[2]Y. X. Zhao, SLAC TN-81-5 (1981).

[3]I. Langmuir, Phys. Rev. 21, 419 (1923).

FIGURE CAPTIONS

Fig. 1. The anode current performances at low voltage (SLAC's S-band klystrons XK-5).

Fig. 2. The perveance performances of the same tubes as Fig. 1.

Fig. 3. The status of the cathode edge (the dashed lines are the corresponding values without considering the edge effect)

(a) The location of the virtual cathode;

(b) The height of the virtual cathode barrier for different anode voltage;

(c) The extracted current density along the surface.

Fig. 4. Idealized edge barrier and equi-potential lines.

Fig. 5. The potential distribution in front of the cathode.

Fig. 6. The relation between normalized coordinate ξ and potential η.

Fig. 7. The distance between the cathode and the virtual cathode z_m versus anode current density j_a as a function of the ratio of the emission current to the anode current.

Fig. 8. The functions $f_1(\eta)$ and $f_2(\eta)$.

Fig. 9. Theoretical curve of the edge current function versus the relative anode voltage.

Fig. 10. The experimental curves of the edge current

(a) Tube XK-5 M433;

(b) A SPEAR tube (inadequate emission).

Fig. 11. The edge current of normal tubes with different heater power

(a) Tube XK-5 M437;

(b) Tube XK-5 M388.

Fig. 12. The anode current performances before and after high voltage RF testing.

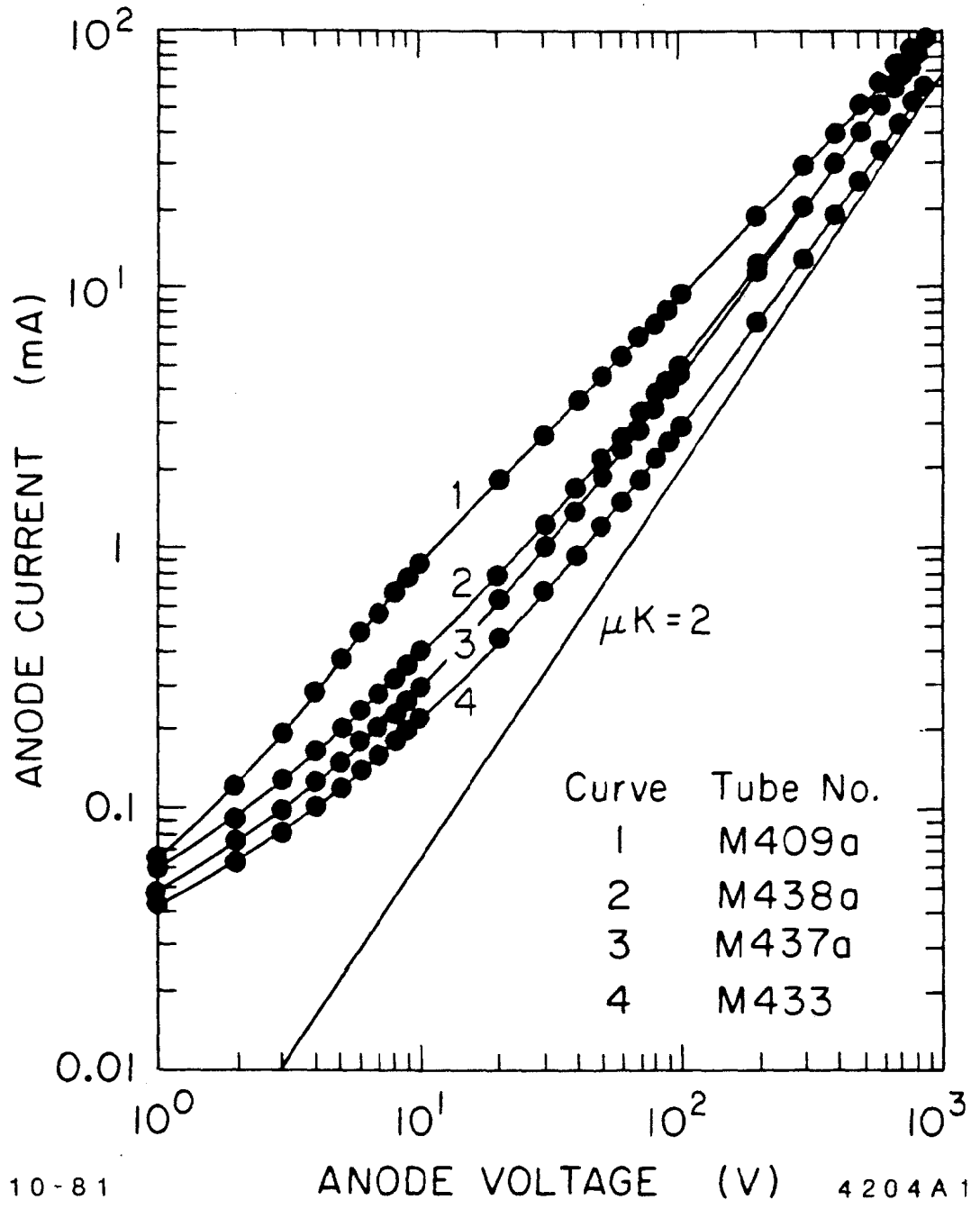
10^2
10^1
1
0.1
0.01
ANODE CURRENT (mA)
10^0
10^1
10^2
10^3
ANODE VOLTAGE (V)
1
2
3
4
$\mu K = 2$
Curve Tube No.
1 M409a
2 M438a
3 M437a
4 M433
10-81
4204A1

Fig. 1

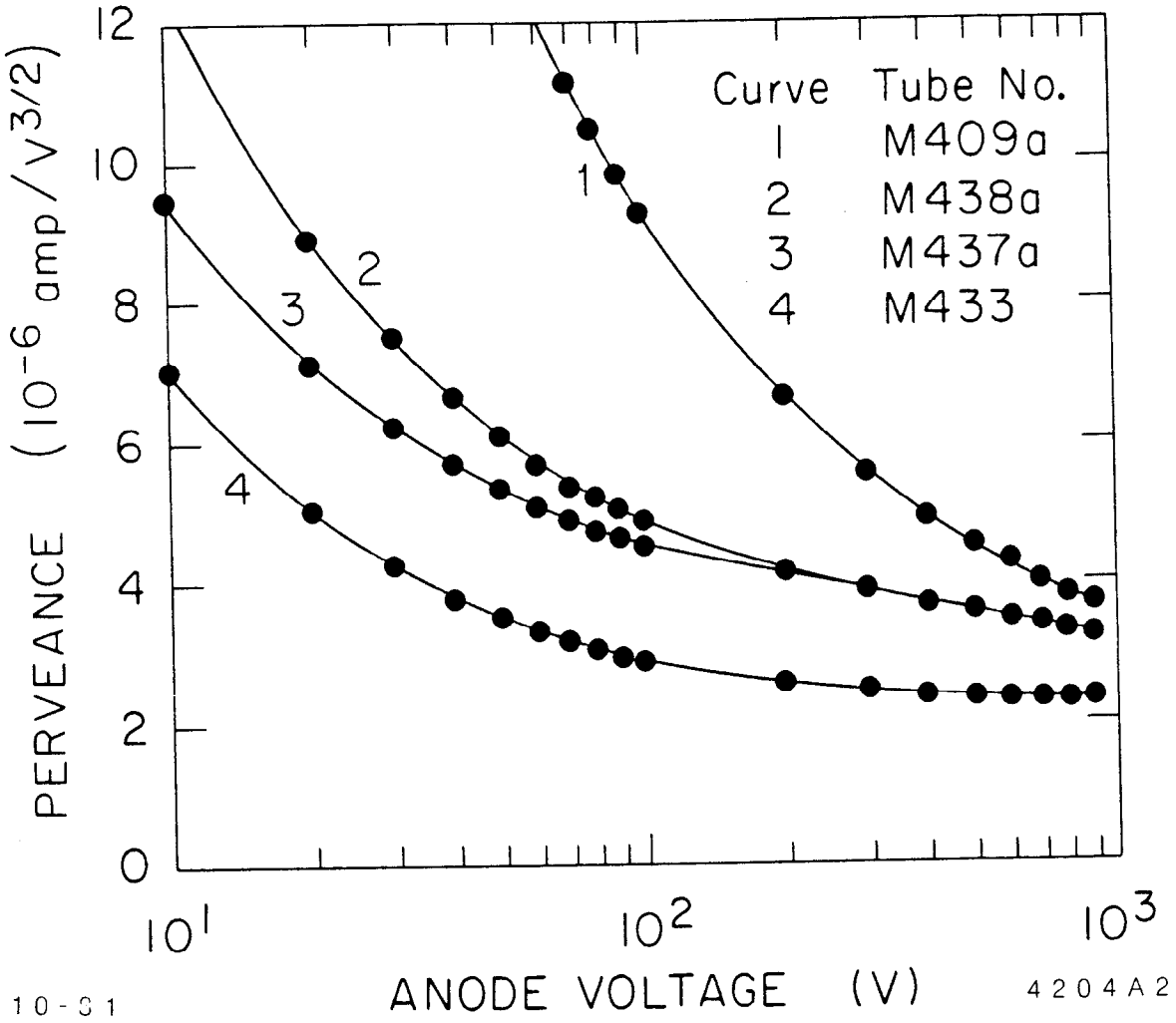
12
10
8
6
4
2
0
PERVEANCE (10⁻⁶ amp/V^3/2)
Curve Tube No.
1 M409a
2 M438a
3 M437a
4 M433
1
2
3
4
10¹
10²
10³
ANODE VOLTAGE (V)
10-31
4204A2

Fig. 2

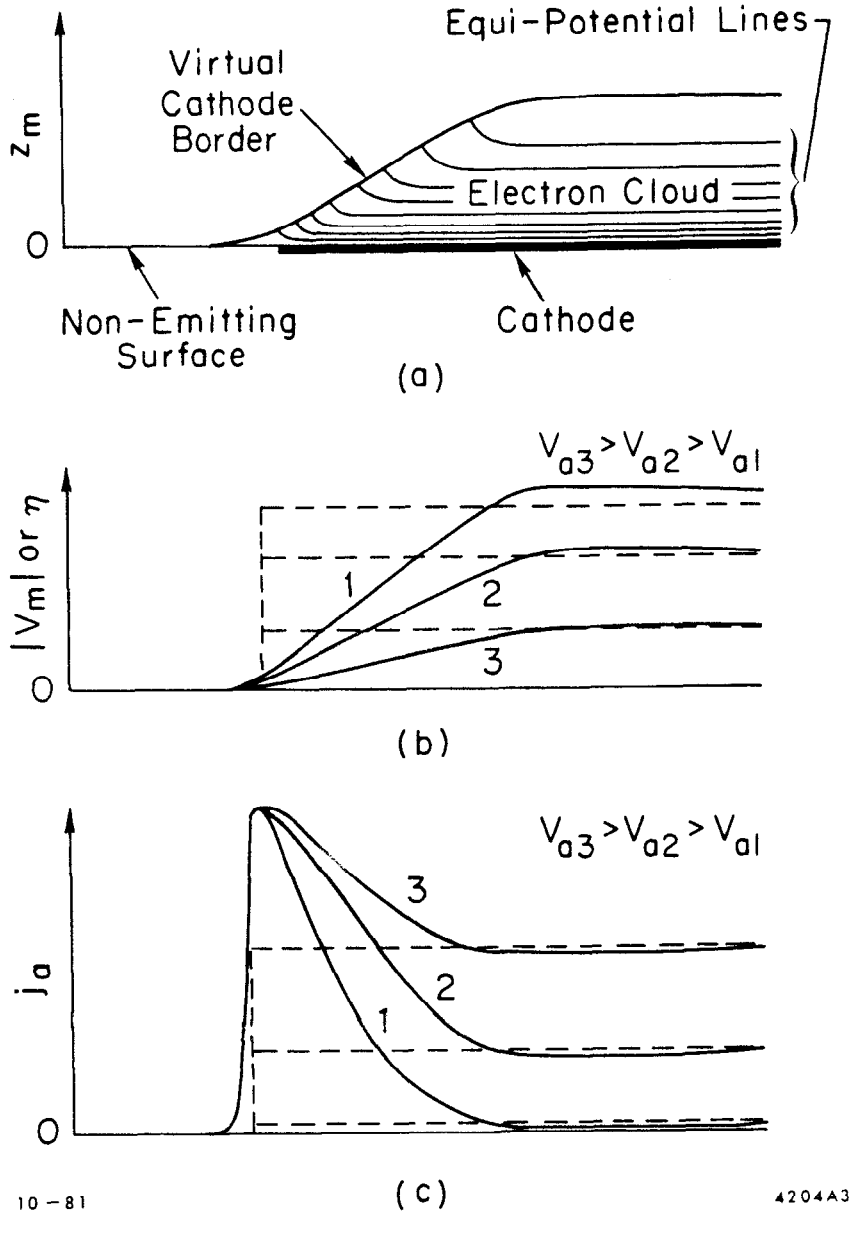
Equi-Potential Lines
Virtual
Cathode
Border
z_m
Electron Cloud
0
Non-Emitting
Surface
Cathode
(a)
$V_{a3} > V_{a2} > V_{a1}$
$|V_m|$ or η
1
2
3
0
(b)
$V_{a3} > V_{a2} > V_{a1}$
j_a
3
2
1
0
10-81
(c)
4204A3

Fig. 3

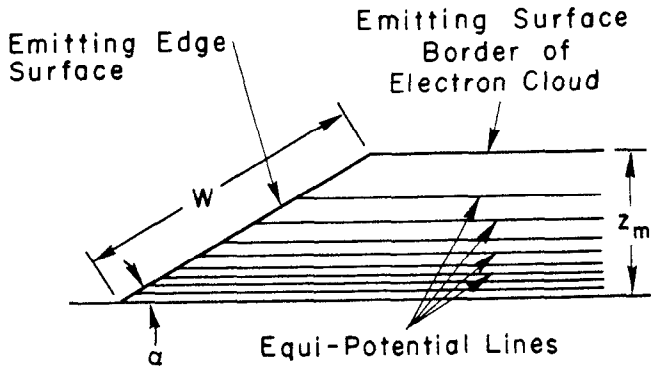
Emitting Edge
Surface
Emitting Surface
Border of
Electron Cloud
W
z_m
a
Equi-Potential Lines
10 – 81
4204A4

Fig. 4

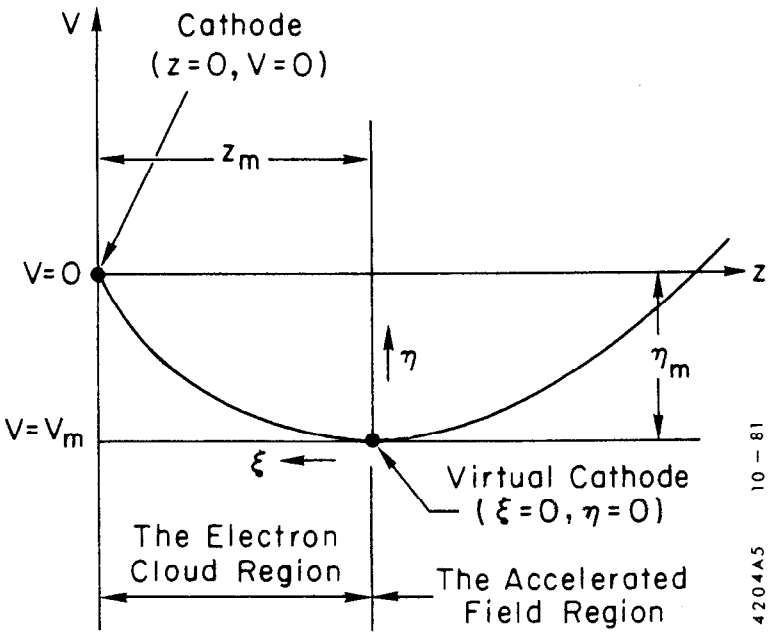
V
Cathode
(z=0, V=0)
z_m
V=0
z
η
η_m
V=V_m
ξ
Virtual Cathode
(ξ=0, η=0)
The Electron
Cloud Region
The Accelerated
Field Region
4204A5 10-81

Fig. 5

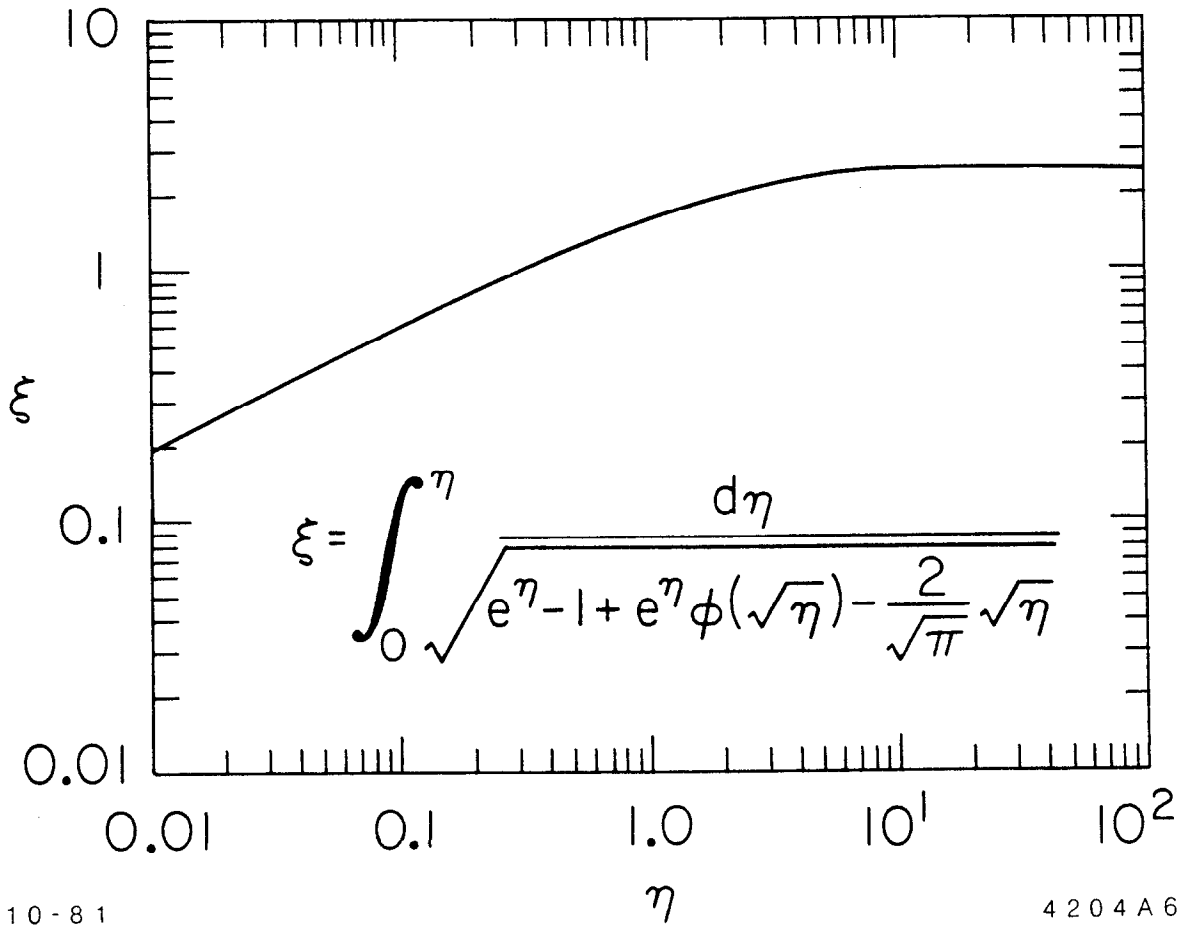
10
1
0.1
0.01
ξ
$\xi = \int_0^{\eta} \frac{d\eta}{\sqrt{e^{\eta} - 1 + e^{\eta}\phi(\sqrt{\eta}) - \frac{2}{\sqrt{\pi}}\sqrt{\eta}}}$
0.01
0.1
1.0
10^1
10^2
η
10-81
4204A6

Fig. 6

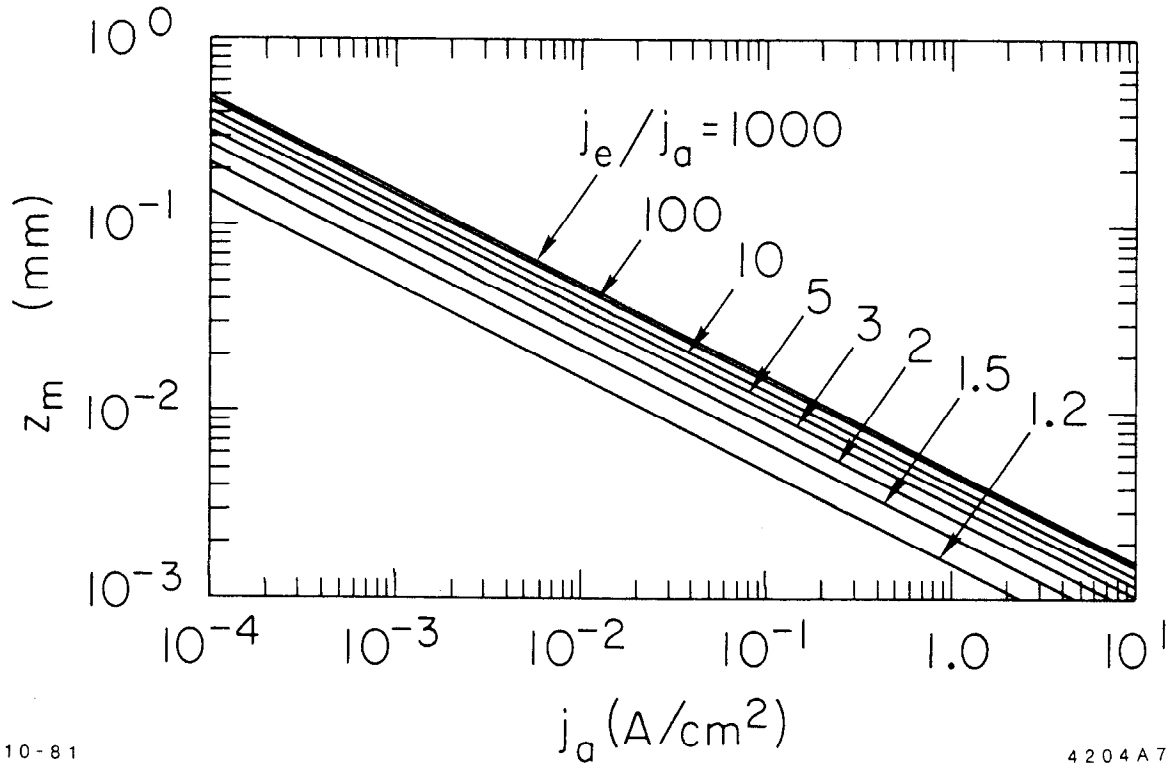
10^0
10^{-1}
10^{-2}
10^{-3}
z_m (mm)
$j_e/j_a = 1000$
100
10
5
3
2
1.5
1.2
10^{-4}
10^{-3}
10^{-2}
10^{-1}
1.0
10^1
j_a (A/cm^2)
10-81
4204A7

Fig. 7

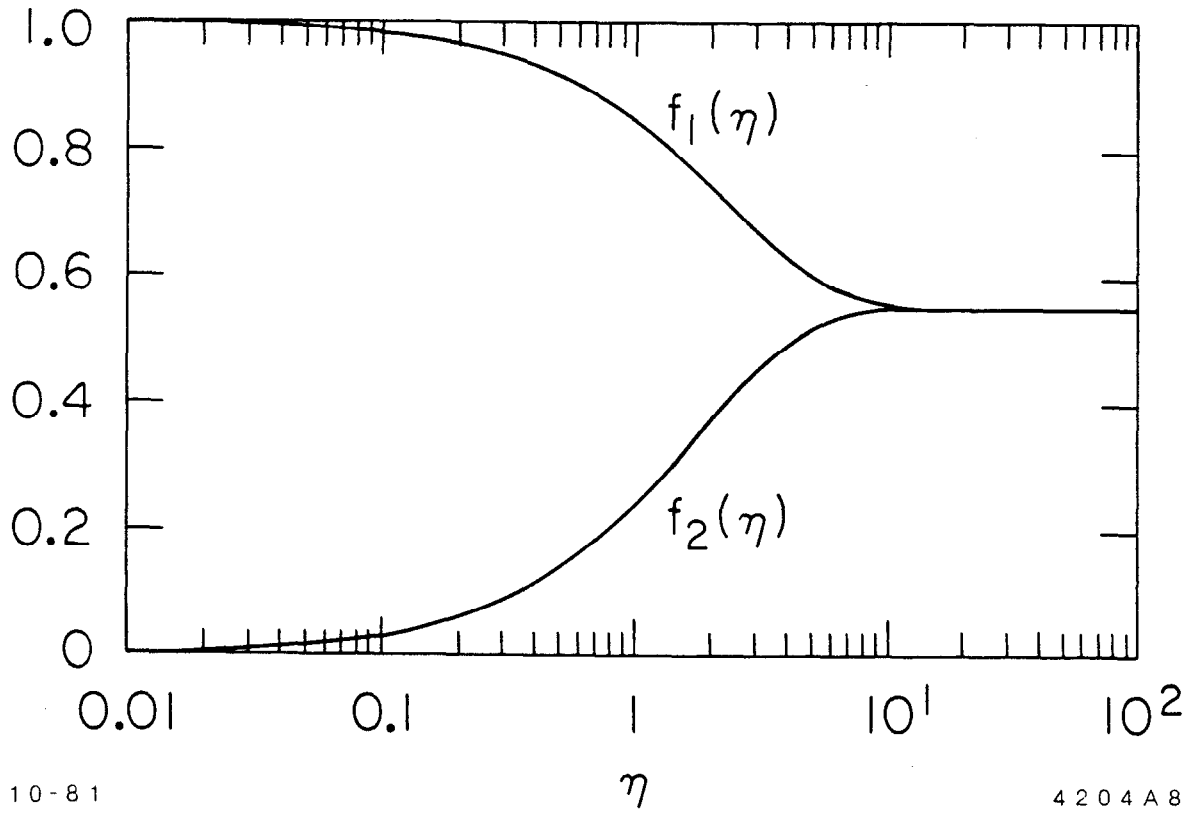

Fig. 8

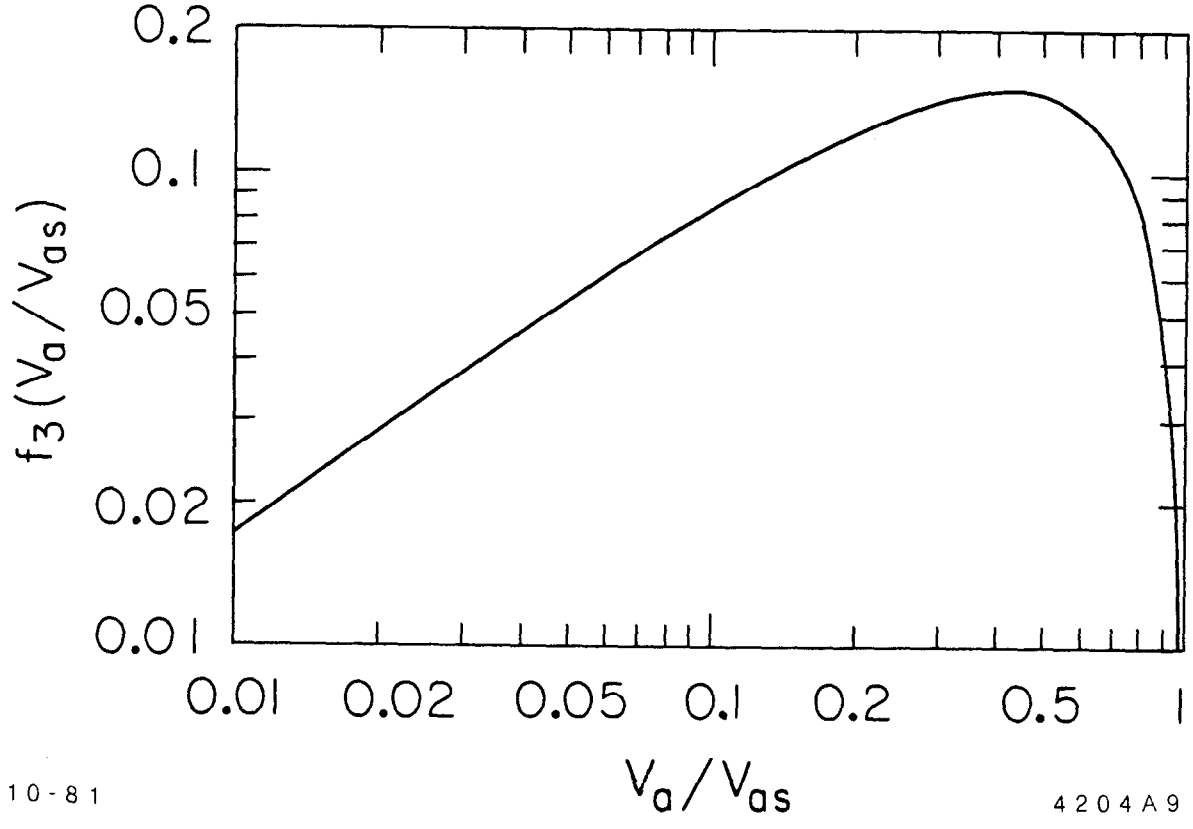
0.2
0.1
0.05
0.02
0.01
$f_3(V_a/V_{as})$
0.01
0.02
0.05
0.1
0.2
0.5
1
V_a/V_{as}
10-81
4204A9

Fig. 9

Tube No. M433

Perveance (μK)	2.11 (Tested)			2.23 (Revised)		
Curve No.	1	2	3	4	5	6
Heater Voltage(V)	15	14	13	12	11	10
Heater Power (W)	223	202	179	157	136	115
Temp at Edge (°C)	687	656	622	590	558	526

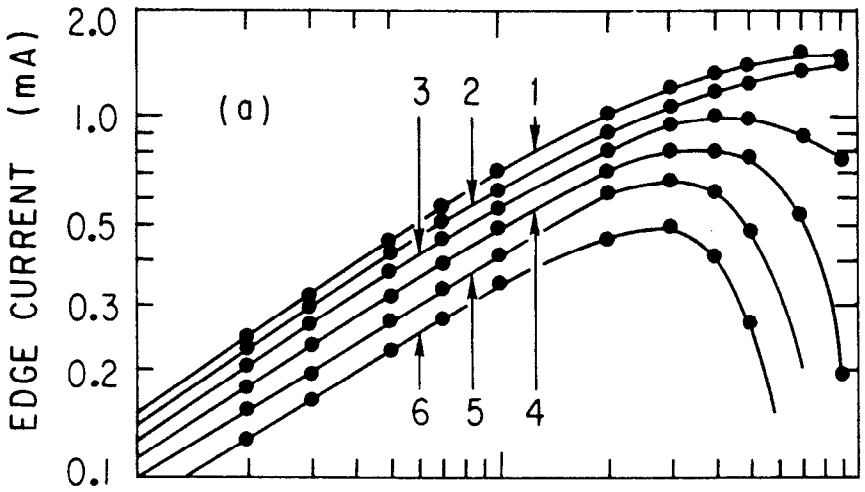

Tube No. (SPEAR)
Perveance (μK) 0.78

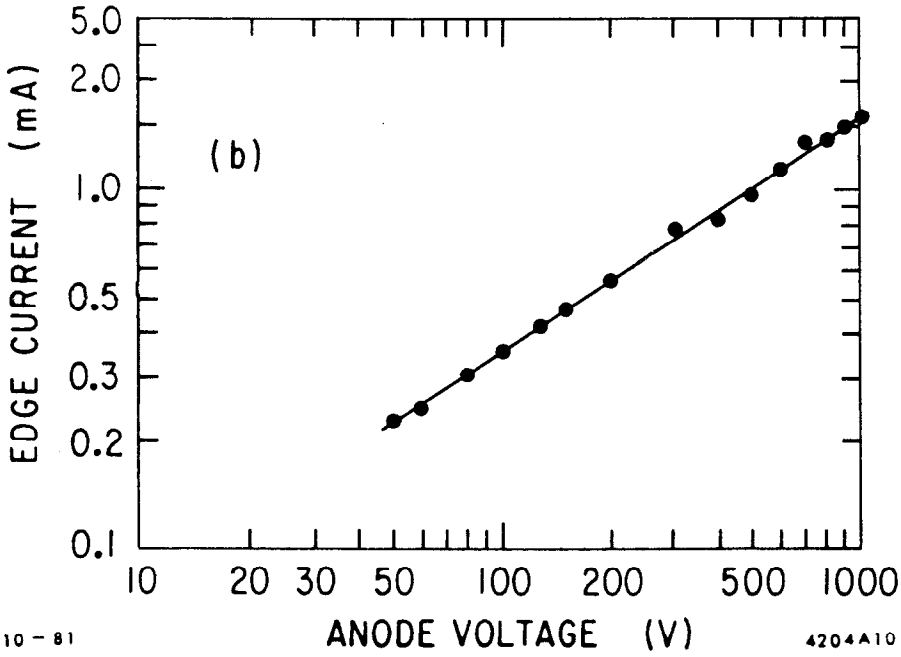

Fig. 10

Tube No. M437

Perveance (μK)	2.08 (Tested)		2.2 (Revised)	
Curve No.	1	2	3	4
Heater Voltage (V)	15	14	13	12
Heater Power (W)	221	195	176	154
Temp at Edge (°C)	684	645	617	584

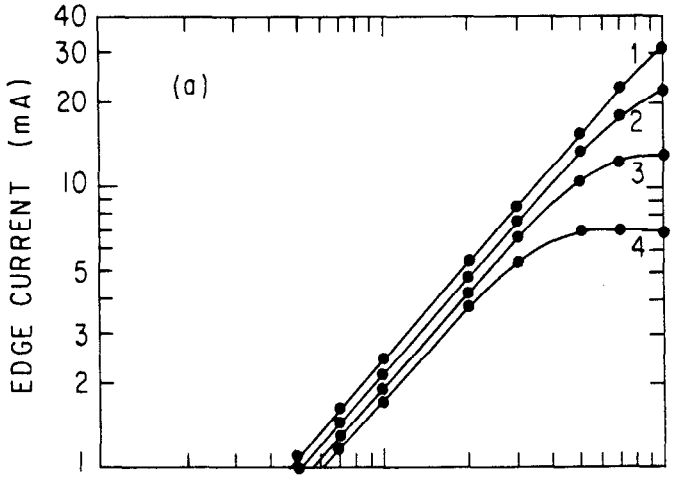

Tube No. M388

Perveance (μK)	2.15 (Tested)			2.27 (Revised)		
Curve No.	1	2	3	4	5	6
Heater Voltage(V)	17	16	15	14	13	12
Heater Power (W)	272	246	221	194	176	154
Temp at Edge (°C)	760	720	684	644	617	584

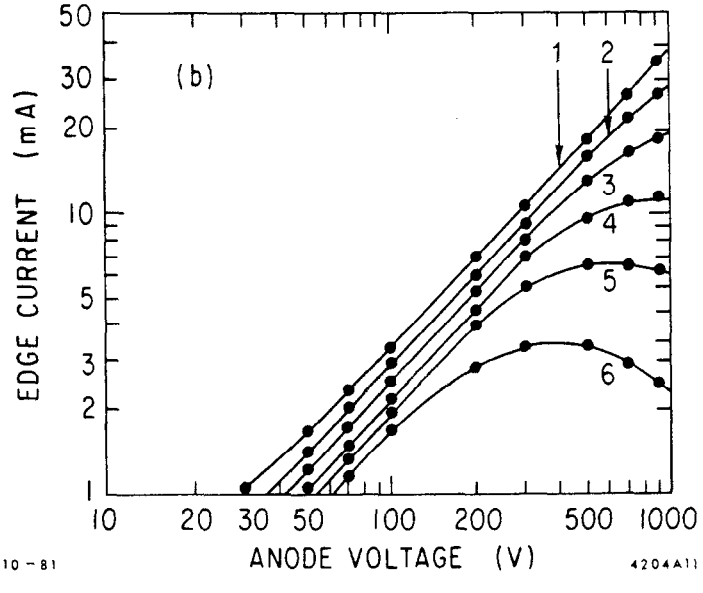

Fig. 11

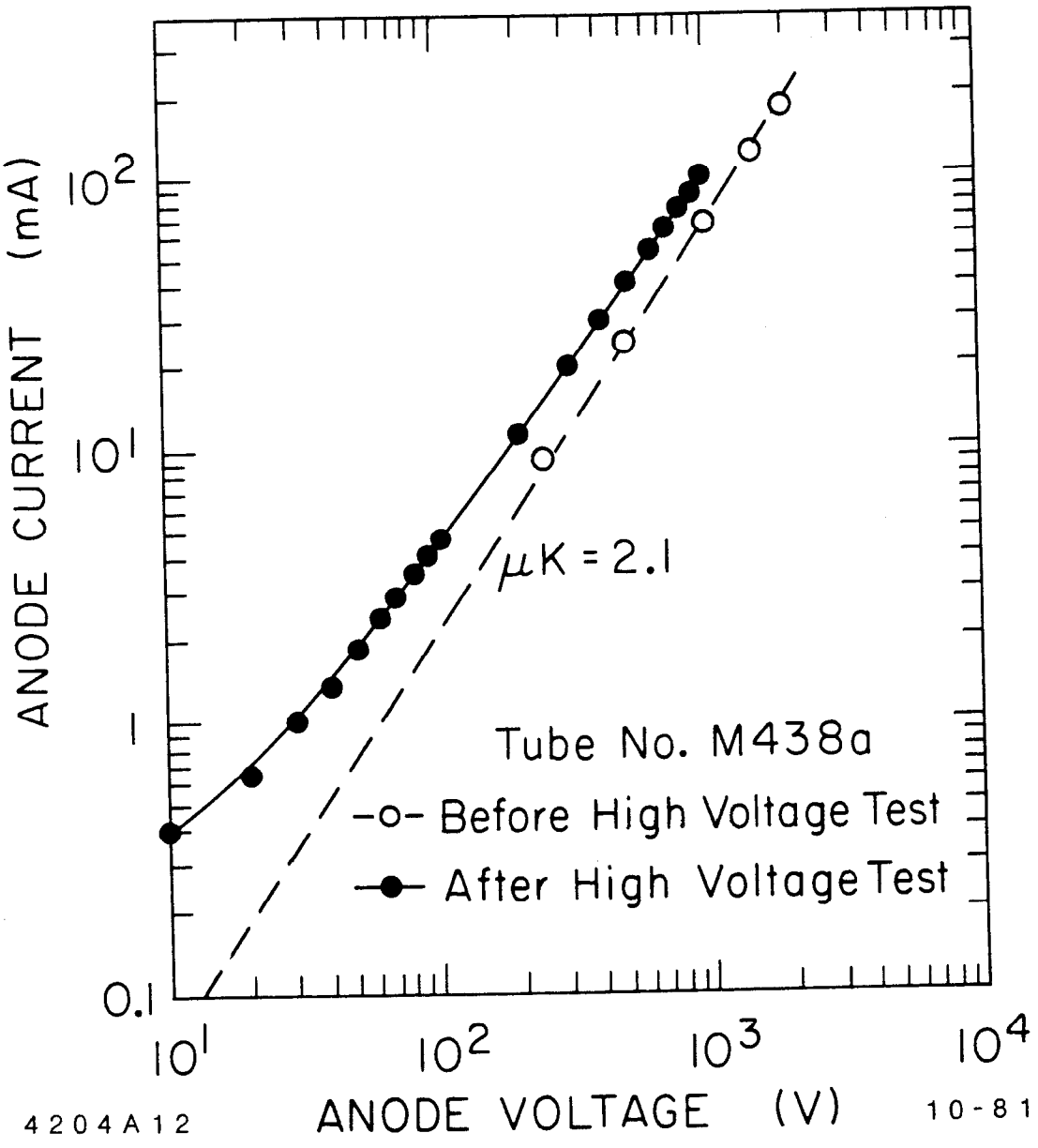
ANODE CURRENT (mA)
10^2
10^1
1
0.1
10^1
10^2
10^3
10^4
ANODE VOLTAGE (V)
$\mu K = 2.1$
Tube No. M438a
-o- Before High Voltage Test
—●— After High Voltage Test
4204A12
10-81

Fig. 12